RSC Advances

PAPER

View Article Online
View Journal | View Issue

Cite this: *RSC Adv.*, 2025, **15**, 33592

Implantation of nano-MOFs into chitosan/sodium alginate hydrogels: boosting the electroanalytical response of chlorogenic acid in food samples

Yang Chong,[a] Limei Ji,[a] Wang Sun[b] and Yang Wang *[b]

Anchoring metal–organic frameworks (MOFs) into flexible carriers to improve the mass-transfer and dispersion properties holds enormous promise in the field of food safety monitoring. Herein, a classical nano-MOF, amino-modified zirconium 1,4-dicarboxybenzene (UiO-66-NH_2), was assembled *via* the solvothermal approach. UiO-66-NH_2 was then implanted into chitosan/sodium alginate hydrogels (CS/SA) to form MOF-based composite hydrogels (CS/UiO-66-NH_2/SA-*x*, *x* indicates the mass ratio of CS/SA, which was set to 1, 2 and 3). Next, an electroanalytical sensing platform (CS/UiO-66-NH_2/SA-2/GCE) was effectively constructed with the CS/UiO-66-NH_2/SA-2-modified glassy carbon electrode (GCE). CS/UiO-66-NH_2/SA-2/GCE achieved an excellent linear detection range (0.1–1000 μmol L^{-1}) and sensitive detection limit (0.03 μmol L^{-1}) for the target analyte chlorogenic acid (CGA), a vital biomolecule in food, under optimal buffer solution conditions. At the same time, the electrochemical sensor presented good anti-interference capability in the presence of a range of ions and biomolecule interferences. During the evaluation of real samples (apple and coffee), the CS/UiO-66-NH_2/SA-2-based electrochemical sensing platform achieved recovery rates of 99.2–103.4%. In short, combining MOF materials with flexible hydrogels offers novel perspectives for the assessment of markers in food.

Received 3rd August 2025
Accepted 1st September 2025

DOI: 10.1039/d5ra05652g

rsc.li/rsc-advances

1 Introduction

Chlorogenic acid (CGA) is a natural polyphenolic compound widely found in coffee beans, apples, tea and other plants.[1,2] Furthermore, chlorogenic acid is formed by the esterification reaction between caffeic acid and quinic acid, and it has significant biological activities, such as antioxidant and anti-inflammatory properties and metabolic regulation.[3–5] It is worth noting that the detection of chlorogenic acid in food is critical for ensuring food quality and safety because its content directly affects the nutritional value and functionality of food, and as an antioxidant, it can delay the oxidative deterioration of food. In addition, chlorogenic acid is susceptible to degradation by temperature and pH variations during processing. Therefore, accurate assessment of chlorogenic acid can not only guide the development of healthy foods and meet consumer demand for functional ingredients but also provide a scientific basis for food labeling and enhance the market competitiveness of products. Compared with high-performance liquid chromatography, spectrophotometry, chemiluminescence and other detection methods, electrochemical analysis has the benefits of easy operation, fast response and high sensitivity;[6,7] therefore, the selection of suitable electrode materials has become the primary problem faced by researchers.

Hydrogels are three-dimensional network structures formed *via* hydrophilic polymer chains through covalent bonding (chemical cross-linking), hydrogen bonding, or van der Waals forces (physical cross-linking), and their pores can store a large amount of water; this unique structure endows hydrogels with high water retention capability and adjustable mechanical properties.[8–10] Special emphasis is placed on the fact that the rich three-dimensional pore-like structure of hydrogels facilitates the diffusion and transport of target molecules. At present, chitosan–sodium alginate (CS–SA)-based hydrogel/composites have attracted widespread attention from scientists owing to their good biocompatibility, environmental friendliness, and electrochemical recognition ability.[11–13] However, the inherent electroanalytical activity of chitosan–sodium alginate hydrogels is relatively weak; therefore, implanting guest materials with superior properties into the hydrogels and thereby improving the signal response of the analytes would be an effective strategy.

Metal–organic frameworks (MOFs) are crystalline materials assembled from metal nodes/clusters with organic ligands.[14] As a classical MOF material, UiO-66-NH_2 presents unique advantages in the electrochemical detection of chlorogenic acid. Specifically, (1) the three-dimensional network structures assembled by metal ions and linkers expose more active centers; (2) the hydrogen bonding or electrostatic interaction

[a]*Department of Clinical Nutrition, The Affiliated Hospital of Yangzhou University, Yangzhou University, Yangzhou, Jiangsu, 225000, China*
[b]*School of Chemistry and Chemical Engineering, Yangzhou University, Yangzhou 225002, China. E-mail: wangyzu@126.com*

between the amino group (–NH_2) of UiO-66-NH_2 and the phenolic hydroxyl group of chlorogenic acid enhances specific adsorption, which significantly improves the selectivity of the target molecules; (3) the rigid structure and chemical stability of the MOF framework can ensure the long-term stable signal response of the modified electrode in complex biological environments, and the π–π conjugation effect of the amino modification can optimize the electron transfer paths.[15–17] Therefore, based on the unique merits of UiO-66-NH_2, it is a prospectively ideal candidate for monitoring the dynamics of chlorogenic acid in metabolic regulation or disease markers in real time.

In this work, a sodium alginate–chitosan composite hydrogel loaded with UiO-66-NH_2 was designed and synthesized, which can be used for the electrochemical detection of chlorogenic acid in food. Multiple hydrogen bonds are formed and electrostatic adsorption occurs within the system due to the interaction of the carboxyl group of sodium alginate and the amino group of chitosan with the amino group of UiO-66-NH_2. The hydrogel material shows significant synergistic advantages in the electrochemical detection of chlorogenic acid: its three-dimensional porous network structure not only provides a uniformly dispersed carrier for UiO-66-NH_2, but also enhances the effective specific surface area and exposure of the active sites. Moreover, the flexible three-dimensional interface of hydrogels facilitates the transport of electrons. By combining the classic UiO-66-NH_2 and the network structure of hydrogels, the constructed electroanalytical sensor can realize the high-sensitivity detection of chlorogenic acid and maintains good anti-interference and reproducibility in complex biological matrices, which provides a valuable reference for the efficient and stable evaluation of chlorogenic acid.

2 Experimental

The chemicals, characterization and calculation equations are available in SI. Meanwhile, the specific synthesis route was shown in Scheme 1.

2.1 Preparation of UiO-66-NH_2

UiO-66-NH_2 was prepared by referring to the previous literature, with modifications.[18] Firstly, 1.0 mmol 2-aminoterephthalic acid and 1.0 mmol $ZrCl_4$ were added to 50 mL DMF solution and stirred vigorously. Thereafter, an appropriate amount of acetic acid was introduced into the above solution, and the mixture was sonicated for half an hour. Finally, the above mixture was transferred to a stainless-steel autoclave lined with polytetrafluoroethylene, and the reaction was carried out at 120 °C for 24 h by a solvothermal method. After the reaction, UiO-66-NH_2 was washed with DMF and anhydrous ethanol, and then stored in a vacuum-oven at 60 °C for 12 h.

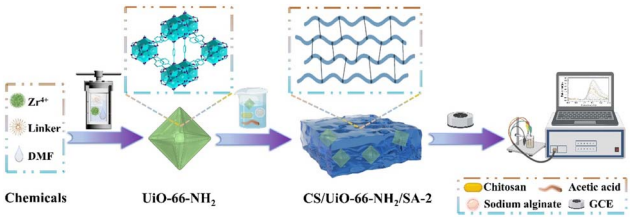

Scheme 1 Schematic of the synthesis route of CS/UiO-66-NH_2/SA-2.

2.2 Preparation of CS/UiO-66-NH_2/SA-x (x = 1, 2, and 3)

Appropriate amounts of chitosan and 0.03 g of UiO-66-NH_2 were added to 20 mL deionized water and stirred for 2 h. Thereafter, sodium alginate was introduced into the above solution and stirring was continued for 3 h. The obtained precursor solution was poured into a mold and placed in a closed environment containing acetic acid (100 μL) to form the hydrogel. Notably, the samples with mass ratios of CS (0.2 g or 0.4 g or 0.6 g) to SA (0.6 g or 0.4 g or 0.2 g) of 1 : 3, 1 : 1 and 3 : 1 were named CS/UiO-66-NH_2/SA-1, CS/UiO-66-NH_2/SA-2 and CS/UiO-66-NH_2/SA-3, respectively. Using the above preparation method, the hydrogel without UiO-66-NH_2 was synthesized and named CS/SA.

3 Results and discussion

3.1 Characterization of materials

As displayed in Fig. 1, the MOF-based hydrogel could be obtained by aging the hydrogel precursor solution in a closed

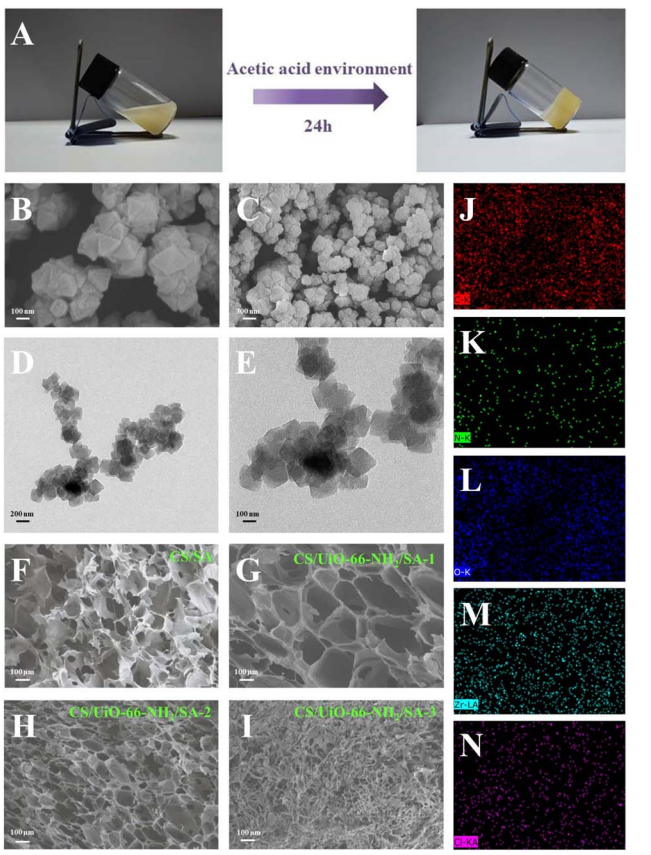

Fig. 1 Physical diagram of the hydrogel formation (A); SEM and TEM images of UiO-66-NH_2 at different magnifications (B)–(E); SEM images of CS/SA, CS/UiO-66-NH_2/SA-1, CS/UiO-66-NH_2/SA-2, and CS/UiO-66-NH_2/SA-3 (F)–(I); and elemental mapping of CS/UiO-66-NH_2/SA-2 (J)–(N).

acidic environment for 24 h. The surface morphology and fine features of the synthesized UiO-66-NH_2 were analyzed *via* SEM and TEM. As depicted in Fig. 1B–E, UiO-66-NH_2 exhibited an octahedral structure with an average length of 200 nm and a width of 120 nm. As shown in Fig. 1F–I, the series of hydrogel materials presented apparent network structures. Notably, the pore size of the hydrogel decreased gradually with increasing chitosan proportion. This may be attributed to the fact that when the proportion of chitosan increases, the functional groups (amino and hydroxyl groups) on the molecular chain provide more crosslinking sites, promoting the physical or chemical crosslinking network to be closer and thereby intensifying the chain entanglement effect and limiting the space for pore expansion.[19] In addition, the high percentage of chitosan solution led to high viscosity, which enhances the intermolecular affinity to some extent, thus facilitating the gelation process and resulting in a denser structure. As can be seen in Fig. 1J–N and S1, the elemental mapping results of CS/UiO-66-NH_2/SA-2 revealed the presence of C, N, O, Zr and Cl elements in the hydrogel with a uniform distribution, suggesting that UiO-66-NH_2 was successfully introduced into the hydrogel. Simultaneously, the specific content of the elements in CS/UiO-66-NH_2/SA-2 is summarized in Table S1.

In this research, contact angle, water content and swelling tests were conducted for the hydrogel or MOF-based hydrogels. As illustrated in Fig. 2A–D, the contact angles of the range of hydrogel samples were in the order: CS/SA > CS/UiO-66-NH_2/SA-3 > CS/UiO-66-NH_2/SA-2 > CS/UiO-66-NH_2/SA-1. The four hydrogel materials all exhibited good hydrophilicity. In the assessment of the water content (Fig. 2E), the water content of CS/UiO-66-NH_2/SA-1 was higher than that of the other hydrogels. As shown in Fig. 3F, the swelling rates of all hydrogels increased sharply in the first 8 hours and then gradually stabilized. This is generally consistent with the trend in the contact angle. The above situation is closely related to the pore size of the hydrogels. In addition, the introduction of MOFs may affect the osmotic pressure within the system to some extent.[20,21] The specific equations for calculating the water content and swelling rate can be found in eqn (S1) and (S2). The synthesized materials were characterized through Fourier-transform infrared spectroscopy (FT-IR) and X-ray diffraction (XRD). The characteristic signal of chitosan (CS) at about 3279 cm^{-1} in Fig. 3A belonged to the stretching vibration peak of the hydroxyl/amino group and the IR signals at 1657 cm^{-1} and 1582 cm^{-1} represent the N–H bending vibration peaks. The IR peaks of sodium alginate (SA) at 1602 cm^{-1} and 1419 cm^{-1} were attributed to the asymmetric and symmetric stretching vibrations of $-COO^-$.[22,23] The broad peak of SA near 3250 cm^{-1} was assigned to the hydroxyl group. As for the MOFs, the IR signal of UiO-66-NH_2 at 3313 cm^{-1} was the stretching vibration peak of N–H. The IR peaks at 1675 cm^{-1} and 1567 cm^{-1} correspond to the bending vibration peak of N–H, and the characteristic peaks at 652 cm^{-1} and 774 cm^{-1} are the stretching or bending vibration peaks of Zr–O. Upon combining UiO-66-NH_2 with the hydrogels, the N–H peak underwent a red-shift, indicating the formation of hydrogen bonds in the composite hydrogel.[24,25] Therefore, there is an interfacial hydrogen bonding interaction between UiO-66-NH_2 and the hydrogel matrix. In addition, the zeta potential data indicate that an electrostatic attraction exists between CS/SA and UiO-66-NH_2 (Fig. S2). With regard to the XRD results (Fig. 3B), there were two characteristic diffraction peaks at 5–10° for UiO-66-NH_2, in agreement with the simulated result (Cambridge Crystallographic Data Centre number, #49-1642).[26] When UiO-66-NH_2 was compounded with the hydrogels, the characteristic peak intensity of the composites was significantly reduced and broad amorphous peaks appeared, indicating that the MOF-based hydrogels were synthesized successfully.[27]

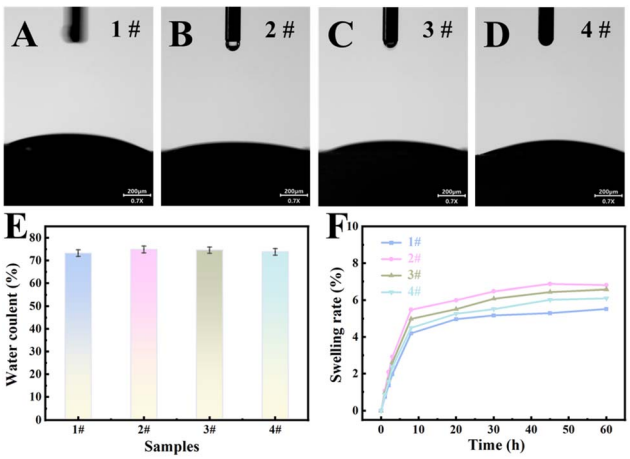

Fig. 2 Contact angles (A)–(D), water contents (E) and swelling rates (F) of CS/SA (1#), CS/UiO-66-NH_2/SA-1 (2#), CS/UiO-66-NH_2/SA-2 (3#) and CS/UiO-66-NH_2/SA-3 (4#).

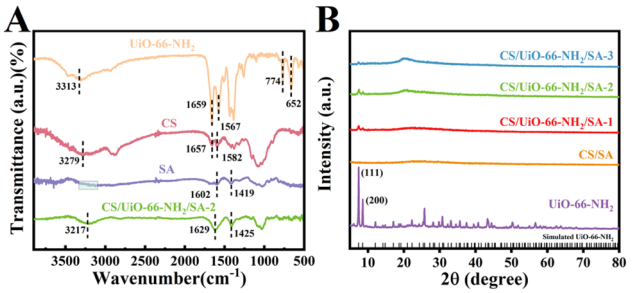

Fig. 3 FT-IR spectra of UiO-66-NH_2, CS, SA and CS/UiO-66-NH_2/SA-2 (A) and XRD profiles of UiO-66-NH_2, CS/SA, CS/UiO-66-NH_2/SA-1, CS/UiO-66-NH_2/SA-2 and CS/UiO-66-NH_2/SA-3 (B).

It can be seen from the XPS broad spectrum given in Fig. 4A that the MOF-based hydrogel was composed of Zr, Na, O, C, N and Cl elements. In the C 1s and N 1s XPS spectra (Fig. 4B and C), the corresponding characteristic XPS peaks (C=C, C–N, O=C–O, C–N and $-NH_3^+$) were observed for CS/UiO-66-NH_2/SA-2. In the Zr 3d spectrum (Fig. 4D), the splitting distance was 2.4 eV, indicating that Zr is in the +4 valence state (Zr^{4+}), which is consistent with the coordination environment of the $[Zr_6O_4(OH)_4]$ cluster in UiO-66-NH_2.[28] The above XPS results indicate that CS/UiO-66-NH_2/SA-2 was successfully constructed. In addition, the formation mechanism of the CS/UiO-66-NH_2/SA

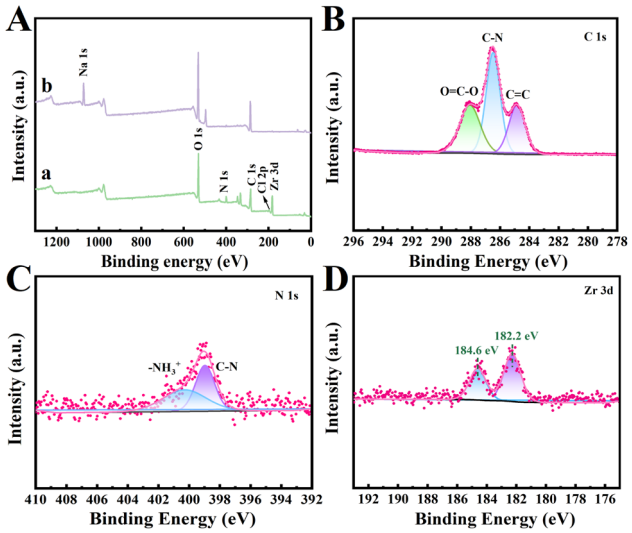

Fig. 4 XPS broad spectrum (A) of UiO-66-NH_2 (a) and CS/UiO-66-NH_2/SA-2 (b) and C 1s (B), N 1s (C), and Zr 3d (D) spectra of CS/UiO-66-NH_2/SA-2.

hydrogel is shown below. Firstly, the UiO-66-NH_2 particles are uniformly dispersed in chitosan solution by ultrasonic or stirring. In the presence of acetic acid at low pH, the amino groups of chitosan and UiO-66-NH_2 are protonated, and the two may reduce the agglomeration by electrostatic repulsion. The carboxyl group of sodium alginate is partially deprotonated, which enhances the interaction between the positive and negative charges. The protonated amino ($-NH_3^+$) of chitosan and UiO-66-NH_2 and the carboxylate ($-COO^-$) of sodium alginate form an ion cross-linked network by electrostatic attraction. At the same time, a hydrogen bond network is formed between the hydroxyl group and amino group of chitosan and the hydroxyl group and carboxyl group of sodium alginate to further stabilize the gel structure. In addition, the UiO-66-NH_2 particles act as physical fillers to enhance the mechanical strength of the network structure through entanglement.

3.2 Evaluation of electrochemical performance of modified electrodes

As shown in Fig. S3, the electrode modified with $ZrCl_4$ or 2-aminoterephthalic acid did not produce a signal response to chlorogenic acid. Of note, when 2-aminoterephthalic acid underwent periodic self-assembly with $ZrCl_4$ to form UiO-66-NH_2, the current signal of chlorogenic acid could be clearly observed from the cyclic voltammetry (CV) curve. The above phenomenon can be attributed to the large specific surface area and porous structure of UiO-66-NH_2,[29,30] which is conducive to the enrichment and diffusion of CGA. As depicted in Fig. 5A, when the CGA solution was not injected in the PBS solution, the CV of the modified electrode did not show a significant signal response at this time. Fig. 5B presents the CV curves of bare GCE, UiO-66-NH_2/GCE, CS/SA/GCE and CS/UiO-66-NH_2/SA-2/GCE in the presence of CGA. Specifically, the oxidation peak current of bare GCE was relatively weak. When the CS/SA

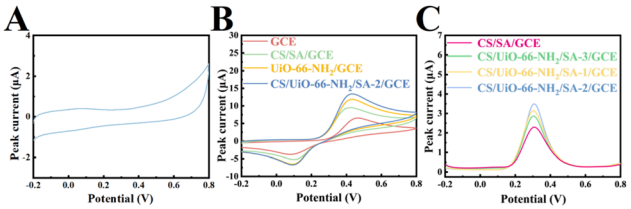

Fig. 5 CV curves of CS/UiO-66-NH_2/SA-2/GCE in PBS solution without CGA (A) and CV curves (B) and DPV curves (C) for a series of modified electrodes in PBS solution containing CGA (pH = 6.0).

hydrogel was modified on the surface of GCE, the intensity of the oxidation peak increased. The peak current of UiO-66-NH_2/GCE was superior to that of CS/SA/GCE. Special emphasis is given to the fact that CS/UiO-66-NH_2/SA-2/GCE presented the maximum peak current value after combining CS/SA and UiO-66-NH_2. The oxidation peak current was 2.32 times, 1.73 times and 1.16 times that of GCE, CS/SA/GCE and UiO-66-NH_2/GCE, respectively. During the detection process, the hydrophilicity and network structure of the hydrogel facilitated electrolyte penetration and electron transfer, providing a stable electrode interface, and the porous structure of UiO-66-NH_2 also facilitated the enrichment of CGA molecules.[31] The effects of different ratios of CS and SA hydrogels on the electroanalytical performance of CGA were also compared using differential pulse voltammetry (DPV). It can be seen from Fig. 5C that as the proportion of chitosan in the hydrogel increased, the peak current first grew and then decreased. In detail, when the ratio of CS and SA was 1 : 1, the signal response of CGA was the strongest. The above phenomenon may be attributed to the fact that excessively loose or dense pores may affect the structural stability as well as the mass transfer efficiency, and thus suitable pores are favorable for CGA detection.

3.3 Optimization of kinetic parameters

Considering that the pH value of the solution may affect the electrochemical performance by regulating electron transfer between the electrode surface and the electrolyte, the signal response of the CS/UiO-66-NH_2/SA-2-modified electrode to CGA was systematically investigated in the pH range of 4.0–8.0. As shown in Fig. 6A, the anodic oxidation peak potential of CGA presented a significant negative shift trend with increasing pH, indicating that there is a direct participation of protons in the electrochemical oxidation reaction of CGA.[32] This is a key proof of the participation of protons in the electroanalytical reaction of CGA. Further analysis revealed a good linear correlation between the peak potential (E_p) and pH (Fig. 6B), with a regression equation of E_p (V) = 0.6944–0.0624 pH (R^2 = 0.9900). The acquired slope (62.4 mV pH^{-1}) is close to the theoretical value (59.0 mV pH^{-1}) of the Nernst equation ($E_p = E^0$ – (0.059 m/n) pH, "m" means protons, "n" means electrons). The ratio of "m" to "n" was calculated to be 1.06 (*i.e.*, m/n ≈ 1). From the above analysis, it can be inferred that CGA transferred the same number (1 : 1) of protons and electrons in the CS/UiO-66-NH_2/SA-2 electrochemical sensing platform.[33] Meanwhile,

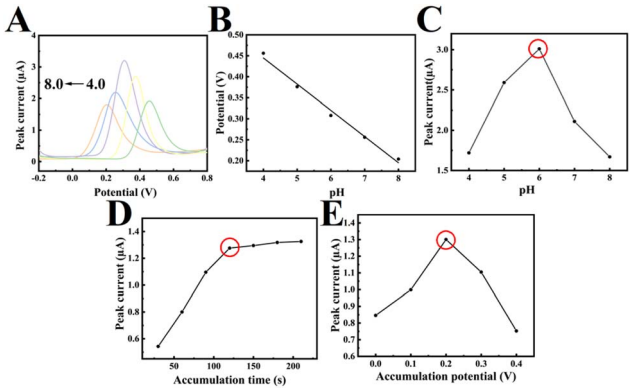

Fig. 6 DPV curves of CS/UiO-66-NH_2/SA-2/GCE in 0.1 mol L^{-1} PBS (pH = 4.0–8.0) solution containing 100 μmol L^{-1} CGA (A); relationship between pH value and potential (B); peak current at different pH values (C); and influence of enrichment time (D) and enrichment potential (E) on peak current of CGA (0.1 mol L^{-1} PBS, pH = 6.0).

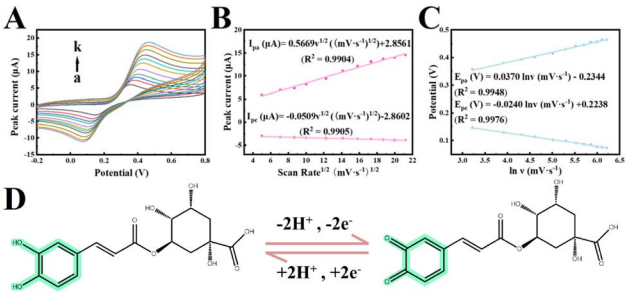

Fig. 7 CV profiles of CS/UiO-66-NH_2/SA-2/GCE for 100 μmol L^{-1} CGA at different scan rates (a–k: 25–450 mV s^{-1}) (0.1 mol L^{-1} PBS, pH = 6.0) (A); linear relationship of oxidation/reduction peak current *vs.* $v^{1/2}$ (B); functional relationship between redox potential and ln *v* (C); and electroanalytical reaction equation of CGA (D).

the intensity of the current response followed a volcano trend with pH, *i.e.*, the peak current reached a maximum at pH = 6.0 (Fig. 6C). Based on the above optimization results, phosphate buffer solution with pH = 6.0 was selected as the medium for detecting CGA in the subsequent experiments to ensure the optimal electrochemical behavior of the constructed electroanalytical sensor. In the research on optimizing the enrichment time and potential, the experimental results show that the above two factors have a certain influence on the signal response of CGA. Specifically, when the time was extended to 120 s (Fig. 6D), the current response gradually increased and stabilized, indicating that the active sites on the electrode surface reached adsorption saturation at this time. Further extension of the time only led to the formation of a concentration gradient in the diffusion layer but did not further improve the enrichment amount. As displayed in Fig. 6E, with a change in the enrichment potential, the current response exhibited a tendency to increase and then decrease, and attained the highest value at 0.2 V. Therefore, 120 s and 0.2 V were finally determined as the best enrichment time and potential, respectively.

In order to further explore the redox reaction kinetics of CGA on the surface of CS/UiO-66-NH_2/SA-2/GCE, the effect of the scan rate on the electrochemical behavior was investigated through CV.[34] As shown in Fig. 7A, the peak oxidation current (I_{pa}) and peak reduction current (I_{pc}) of CGA continuously increase with increasing scan rate in the interval of 25–450 mV s^{-1}. Fig. 7B indicates that there is a good linear relationship between I_{pa} and I_{pc} and the square root of the scan rate ($v^{1/2}$); the regression equations are: I_{pa} (μA) = 2.8561 + 0.5669 $v^{1/2}$ (R^2 = 0.9904); I_{pc} (μA) = −2.8602–0.0509 $v^{1/2}$ (R^2 = 0.9905). This typical feature indicates that the kinetics of the redox reaction of CGA on the electrode interface are mainly dominated by diffusion control. At the same time, this study also observed a significant effect of the scanning rate on the position of the peak potential. With increasing scanning rate, the oxidation peak potential (E_{pa}) gradually shifted to the positive potential direction, while the reduction peak potential (E_{pc}) shifted to the negative potential direction. The above phenomenon can be attributed to the limitation of the electron transfer rate in the electrode reaction. When the scanning rate increases, the irreversibility of the electron transfer process is enhanced, resulting in an increase in the potential difference (ΔE_p) between the oxidation peak and the reduction peak, which further reveals the quasi-reversible characteristics of the reaction CGA on the surface of the modified electrode. Analysis of the related data shows a good linear relationship between the peak potential and ln *v* (Fig. 7C). The specific equations are as follows: E_{pa} (V) = 0.0370 ln *v* + 0.2344 (R^2 = 0.9948); E_{pc} (V) = −0.0240 ln *v* + 0.2238 (R^2 = 0.9976). Furthermore, based on the Laviron equation (eqn (S3)),[35] the number of electrons transferred in the system was calculated to be 2.13 ($n \approx 2$), *i.e.*, two electrons are transferred during the oxidation of CGA. Based on the above, protons and electrons participated in the electroanalytical reaction of CGA and the same number of protons and electrons were transferred in this reaction. Therefore, it can be confirmed that 2 electrons and 2 protons were transferred in the electroanalytical reaction of CGA. In summary, the electroanalytical reaction of CGA is a synergistic process driven by electron transfer coupled with proton transfer. Notably, in order to facilitate understanding of the electroanalytical behavior of the target molecules, Fig. 7D presents the equation for the reaction of CGA on CS/UiO-66-NH_2/SA-2/GCE.

3.4 Quantitative analysis of CGA using CS/UiO-66-NH_2/SA-2/GCE

The current response of CS/UiO-66-NH_2/SA-2/GCE to different concentrations of CGA under the optimized detection conditions is shown in Fig. 8A. When the concentration of CGA was in the range of 0.1–1000 μmol L^{-1}, the oxidation peak current was significantly correlated with the concentration in two linear ranges (Fig. 8B). The corresponding linear regression equations are as follows: I_{pa} (μA) = 0.0307 + 0.0046C (C: 0.1–100 μmol L^{-1}, R^2 = 0.9956); I_{pa} (μA) = 0.2382 + 0.0027C (C: 100–1000 μmol L^{-1}, R^2 = 0.9975). Of note, the difference in the slope of the calibration curve in the low *versus* high concentration ranges can be attributed to the dynamic transformation of the electrochemical reaction mechanism. At low concentrations of CGA

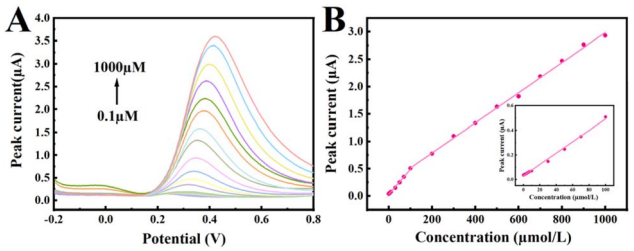

Fig. 8 DPV signals of CGA on CS/UiO-66-NH_2/SA-2/GCE in 0.1 mol L^{-1} PBS (pH = 6.0) (A) and linear plot of current *versus* CGA concentration (B); inset: linear curve at low concentrations (0.1–100 μmol L^{-1}).

(0.1–100 μmol L^{-1}), the CGA molecules are adsorbed on the metal nodes of UiO-66-NH_2 and the active sites of the amino functional groups of chitosan, forming a local enrichment effect. At this time, the adsorption controlled process is dominant. With increasing concentration (100–1000 μmol L^{-1}), the active sites on the electrode surface are gradually covered by the CGA molecules, at which time the mass transfer rate is limited to a certain extent, leading to a shift of the reaction kinetics to diffusion control. In this stage, the CGA molecules in solution need to overcome the interfacial diffusion barrier to reach the reaction sites, hence leading to a decrease in the sensitivity.

Based on the 3S/N (signal-to-noise) principle, the limit of detection (LOD) of CS/UiO-66-NH_2/SA-2/GCE for CGA was 0.03 μmol L^{-1}. In addition, the sensitivity was determined as (0.06 μA μM^{-1} cm^{-2}) based on the ratio of the linear slope to the electrochemical active area (using the Randles–Sevcik equation).[36] In terms of the in-depth mechanism underlying the performance advantages, the CS/UiO-66-NH_2/SA-2 electroanalytical sensor presents a multi-dimensional synergistic enhancement effect. Firstly, the large specific surface area and porous structure of UiO-66-NH_2 are conducive to the enrichment and diffusion of CGA.[37] Secondly, the three-dimensional network of the hydrogel was formed through the combined with the electrostatic attraction of the amino functional group of CS to the CGA carboxylic acid group, the enrichment ability to the target molecules is significantly improved, while dispersing the UiO-66-NH_2. Finally, the multiple molecular interactions (π–π stacking, hydrogen bonding and electrostatic interaction) of CGA with the MOFs and hydrogels in the system can enhance the adsorption efficiency of CGA. To sum up, the triple synergistic effect significantly improved the electrochemical response signal of CGA.

3.5 Evaluation of repeatability, stability and anti-interference

In addition to the quantitative analysis of CGA using the CS/UiO-66-NH_2/SA-2 electrochemical sensing platform, exploring the repeatability, reproducibility and stability is equally important. In the repeatability test (Fig. 9A), a single CS/UiO-66-NH_2/SA-2 electrode was used to detect CGA ten consecutive times; the acquired current signal fluctuated only slightly in these experiments. The relative standard deviation of the peak current was 1.08%, which proves that the electrode surface is

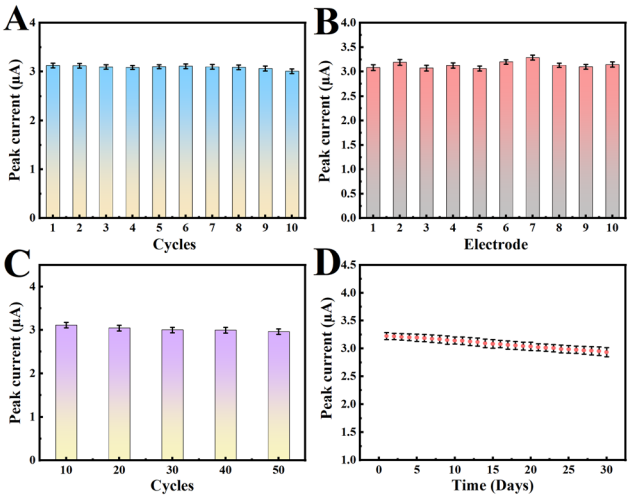

Fig. 9 Repeatability evaluation of the CS/UiO-66-NH_2/SA-2-based electroanalytical sensor (A); analysis of the reproducibility of CS/UiO-66-NH_2/SA-2/GCE with 10 independent electrodes (B); cyclic stability (C) and storage stability (D) of CS/UiO-66-NH_2/SA-2/GCE (0.1 mol L^{-1} PBS, pH = 6.0).

not passivated in the multiple redox reactions. As for the reproducibility assessment (Fig. 9B), the CGA molecule was detected using ten batches of independently prepared working electrodes. The obtained relative standard deviation of the peak current was only 2.23%, indicating that this sensor has good reproducibility. In the assessment of the cyclic stability (Fig. 9C), after several consecutive scans, the peak current of CS/UiO-66-NH_2/SA-2/GCE remained at 95.2% of the initial value. In addition, the long-term stability test further verified the reliability of the electrochemical sensor (Fig. 9D). Specifically, the current response of the modified electrode to CGA remained 91.0% of the initial level after storage at 4 °C for 30 days. The stability mechanism can be analyzed as follows: the rigid framework of UiO-66-NH_2 and the flexible network of CS/SA form a 'rigid and flexible' composite structure, which can not only resist the swelling deformation caused by the hot and humid environment, but also buffer the stress damage caused *via* the temperature fluctuation. In addition, the positively charged layer formed by protonation of the amino group of CS in the acidic medium can repel positively charged impurity ions (such as metal cations) in the solution, thereby reducing the risk of contamination on the electrode surface. As shown in Table S2, compared with the CGA sensors reported in the literature,[38–46] CS/UiO-66-NH_2/SA-2/GCE has a low detection limit (0.03 μmol L^{-1}) and a wide linear detection range (0.1–1000 μmol L^{-1}). Briefly, these characteristics make it have important application potential in the fields of food quality monitoring, analysis of the active ingredients in Chinese medicinal materials and the industrial production of natural products. In the future, by adjusting the pore size distribution of UiO-66-NH_2 and crosslinking degree of SA, the mass transfer kinetics and interfacial charge transfer efficiency can be further optimized, and the transformation of the sensor from laboratory research to actual detection scenarios can be realized.

In order to systematically evaluate the selectivity of CS/UiO-66-NH_2/SA-2/CGE for CGA detection, several classical interfering substances (*e.g.*, metal ions and biomolecules) were chosen in this study to assess the anti-interference abilities of the electroanalytical sensing platform. It is particularly emphasized that the selection of interfering species is based on various substances that are similar in structure to CGA or may coexist in the actual samples. This experiment utilizes the DPV technique for analysis of the interference selectivity of the CS/UiO-66-NH_2/SA-2 electrochemical sensor. In this experiment, 100-fold concentrations of dopamine (DA), glucose (Glu), levodopa (L-DOPA), norepinephrine (NE), homovanillic acid (HVA), catechol (CA), uric acid (UA), glutamic acid (GA) and L-cysteine (L-Cys) and 50-fold concentrations of Na^+, Mg^{2+}, Ca^{2+}, K^+, NH_4^+, NO_3^-, PO_4^{3-}, Cl^- and SO_4^{2-} were added to 100 μmol L^{-1} CGA solution to explore their effects on the detection signal. The experimental results (Fig. 10) revealed that the current change rate caused by all the interferences is less than 5%, which fully proves that the fabricated electroanalytical sensor has a high specific recognition ability for CGA. In this study, a number of common biomolecules (quercetin (QU), baicalin (BA), luteolin (LU), ascorbic acid (AA), citric acid (CIA), salicylic acid (SA), *tert*-butylhydroquinone (TB)) that may coexist with chlorogenic acid (CGA) were also selected for anti-interference experiments. Similarly, the concentration of interfering substances was approximately 100 times that of CGA (100 μmol L^{-1}). As displayed in Fig. S4, the CS/UiO-66-NH_2/SA-2 electrochemical sensor could still achieve 85.1% signal response in the presence of a series of interfering substances. The above experimental results indicate that the CS/UiO-66-NH_2/SA-2-based electroanalytical sensing platform possesses good anti-interference properties. The excellent anti-interference characteristics may be related to the following factors: the three-dimensional network structure of the hydrogels can serve as a physical barrier, restricting large molecules or interfering substances with "electrostatic repulsion" from approaching the electrode surface, and only allowing small molecule targets to freely diffuse.

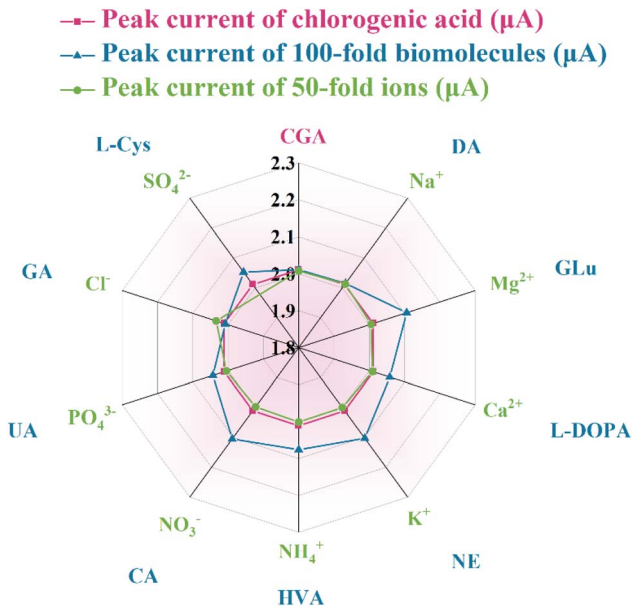

Fig. 10 Radar plot showing the impact of different types of interferences on the CGA response in 0.1 mol L^{-1} PBS (pH = 6.0) using CS/UiO-66-NH_2/SA-2/CGE.

3.6 Evaluation of actual samples

Using the optimal experimental parameters, this study also explores the feasibility of the CS/UiO-66-NH_2/SA-2 electrochemical sensor in the evaluation of real samples. Specifically, commercially available apple and coffee were used as models for the analysis of actual samples, and the means of assessment was chosen to be the spiked recovery experiment. The process for pre-treatment of the samples is shown below. The apples were cored, mashed and dried in an oven at 60 °C for 24 h. Thereafter, 2.5 g of the dried apples was extracted with 20 mL of ethanol at room temperature for 2 h. The supernatant was obtained by centrifugation and diluted to 50 mL. For the coffee samples, 5.0 g of ground coffee was dissolved in 50 mL of PBS aqueous solution and stirred to form a homogeneous coffee solution. It is important to note that all actual samples were filtered through a filter membrane prior to electrochemical evaluation to exclude additional interferences. The results displayed Table S3 show that the recoveries of CGA in the real samples ranged from 99.2% to 103.4% and the relative standard deviation was less than 3% (n = 3). Taken together, the above-mentioned outcomes indicate that the developed electroanalytical sensing platform can be applied for the quantitative analysis of CGA in food samples.

4 Conclusions

In this study, a novel three-dimensional cross-linked network of MOF-based hydrogel composite materials (CS/UiO-66-NH_2/SA-x, x = 1, 2 and 3) was constructed by combining amino-functionalized MOFs (UiO-66-NH_2) with chitosan and sodium alginate. The CS/UiO-66-NH_2/SA-2-based electroanalytical sensing platform demonstrated an excellent linear detection range (0.1–1000 μmol L^{-1}) and detection limit (0.03 μmol L^{-1}, S/N = 3) in the electrochemical detection of chlorogenic acid. The excellent electroanalytical behavior can be attributed to the large specific surface area and porous structure of UiO-66-NH_2, while the three-dimensional network structure of the hydrogel provides good mass transfer, dispersion and enrichment abilities. In addition, for real sample testing, the developed electroanalytical sensing platform also displayed outstanding implementability, and the relative standard deviation was less than 3%. To sum up, this research offers a meaningful reference for the advancement of MOF-based hydrogels in the field of electrochemical analysis.

Author contributions

Yang Chong: methodology, data supervision, writing – original draft. Limei Ji: validation, investigation. Wang Sun: software. Yang Wang: funding acquisition, formal analysis, resources.

Conflicts of interest

All the authors declare no conflict of interest.

Data availability

All underlying data are available within the article and its SI. Supplementary information: Reagents, electrode modification procedures, equation descriptions, and XRD, EDS, SEM, TEM, FT-IR, XPS characterization of the samples as well as electrochemical performance testing. See DOI: **https://doi.org/10.1039/d5ra05652g**.

Acknowledgements

The research was supported by the National Natural Science Foundation of China (No. 22174124), Top-notch Academic Programs Project of Jiangsu Higher Education Institutions (TAPP), and Priority Academic Program Development of Jiangsu Higher Education Institutions (PAPD).

References

1 Z. J. Zhang, X. Han, L. S. Wang, B. L. Wang, Y. H. Huang, M. Ahmad, Z. T. Huang, A. Badshah and W. Sun, *Microchem. J.*, 2024, **207**, 111877.
2 L. W. Chen, N. N. Lu and L. Wang, *Analyst*, 2025, **150**, 447–459.
3 E. Beyyavaş and M. Aslanoglu, *Food Chem.*, 2023, **426**, 136600.
4 J. H. Huang, M. X. Xie, L. He, X. P. Song and T. Z. Cao, *Front. Pharmacol.*, 2023, **14**, 1218015.
5 A. Ponder, K. Krakówko, M. Kruk, S. Kuliński, R. Magoń, D. Ziółkowski, E. Jariene and E. Hallmann, *Molecules*, 2025, **30**, 1290.
6 D. Thatikayala, M. T. Noori, K. R. Riyamol, K. K. Sadasivuni and B. Min, *Coord. Chem. Rev.*, 2025, **540**, 216783.
7 W. Hu, D. L. Jiang, C. Chen, Y. R. Zhou, S. D. Zhang, N. Zhang and L. F. Wang, *Trends Food Sci. Technol.*, 2025, **161**, 104983.
8 D. Thirumalai, M. Santhamoorthy, S. Kim and H. Lim, *Gels*, 2024, **10**, 459.
9 J. Fu, *J. Polym. Sci.*, 2022, **60**, 2605–2606.
10 H. D. Wu, Y. C. Wu, J. Yan, W. Xiao, Y. Q. Wang, H. C. Zhang, X. W. Huang, H. G. Xue, L. Wang, L. C. Tang, Y. W. Mai and J. F. Gao, *Chem. Eng. J.*, 2024, **488**, 150963.
11 J. Li, L. A. Li, Y. Yu, R. X. Qin, C. Y. Yu, C. Chen, Y. M. Dong, Y. D. Tan, Y. N. Liu and X. L. Liu, *Front. Pharmacol.*, 2025, **16**, 1526828.
12 V. Raj, C. J. Raorane, D. Shastri, S. C. Kim and S. Lee, *Int. J. Biol. Macromol.*, 2024, **261**, 129774.
13 H. B. Pei, F. Chen, X. H. Niu, Q. Q. Jia, R. B. Guo, N. J. Liu and Z. L. Mo, *J. Electroanal. Chem.*, 2021, **895**, 115525.
14 Y. Wang, H. H. Chen, X. Y. Hu and H. Yu, *Analyst*, 2016, **141**, 4647–4653.
15 X. J. Wang, G. R. Yang, G. D. Chai, M. S. Nasir, S. L. Wang, X. Zheng, C. Y. Wang and W. Yan, *J. Hydrogen Energy*, 2020, **45**, 30634–30646.
16 Y. Wang, L. Wang, W. Huang, T. Zhang, X. Y. Hu, J. A. Perman and S. Q. Ma, *J. Mater. Chem. A*, 2017, **5**, 8385–8393.
17 W. Pan, W. Q. Wang, P. Wang, D. Chen, S. Liu, L. K. Zhang, Z. Y. Wang, H. Yang, Y. Y. Xie, F. F. Huang, G. H. Zhou and B. Wang, *Mater. Design*, 2024, **238**, 112688.
18 Z. Yuan, L. Zhang, S. Z. Li, W. N. Zhang, M. Lu, Y. Pan, X. J. Xie, L. Huang and W. Huang, *J. Am. Chem. Soc.*, 2018, **140**, 15507–15515.
19 J. Y. Liu, G. R. Sun, W. Sun, X. Q. Zha, N. Wang and Y. Wang, *J. Colloid Interface Sci.*, 2024, **671**, 423–433.
20 Y. P. Liang, B. J. Chen, M. Li, J. H. He, Z. H. Yin and B. L. Guo, *Biomacromolecules*, 2020, **21**, 1841–1852.
21 B. Yang, J. L. Song, Y. H. Jiang, M. Li, J. J. Wei, J. J. Qin, W. J. Peng, F. L. Lasaosa, Y. Y. He, H. L. Mao, J. Yang and Z. W. Gu, *ACS Appl. Mater. Interfaces*, 2020, **12**, 57782–57797.
22 Y. N. Song, S. Li, H. F. Chen, X. Y. Han, G. J. Duns, W. Dessie, W. F. Tang, Y. M. Tan, Z. D. Qin and X. F. Luo, *Int. J. Biol. Macromol.*, 2023, **233**, 123532.
23 Q. K. Zhong, Z. Y. Wu, Y. Q. Qin, Z. Hu, S. D. Li, Z. M. Yang and P. W. Li, *Membranes*, 2019, **9**, 11.
24 A. A. Ehrhard, L. Gunkel, S. Jäger, A. C. Sell, Y. Nagata and J. Hunger, *ACS Catal.*, 2022, **12**, 12689–12700.
25 Y. N. Song, S. Li, H. F. Chen, X. Y. Han, G. J. Duns, W. Dessie, W. F. Tang, Y. M. Tan, Z. D. Qin and X. F. Luo, *Int. J. Biol. Macromol.*, 2023, **233**, 123532.
26 X. Fang, S. B. Wu, Y. H. Wu, W. Yang, Y. L. Li, J. Y. He, P. D. Hong, M. X. Nie, C. Xie, Z. J. Wu, K. S. Zhang, L. T. Kong and J. H. Liu, *Appl. Surf. Sci.*, 2020, **518**, 146226.
27 G. R. Sun, W. Sun, J. Y. Liu, X. Q. Zha, S. Lu and Y. Wang, *Inorg. Chem.*, 2024, **63**, 17263–17273.
28 J. Q. Wang, Z. Y. Li, H. Y. Zhang, W. Wu, Y. Wu, M. Z. Liu, Y. H. Ao and M. Li, *J. Environ. Chem. Eng.*, 2023, **11**, 111488.
29 Q. Q. Zhu, H. W. Zhang, R. R. Yuan and H. M. He, *J. Mater. Chem. C*, 2020, **8**, 15823–15829.
30 Z. S. Li, X. Y. Zhang, Y. Luo, Q. Li, Y. Qin, G. Wang, S. C. Yang and Z. Y. Liu, *Chem. Phys. Lett.*, 2023, **830**, 140825.
31 X. Huang, X. H. Fan, A. M. Li, Y. C. Tian and D. W. Li, *Sci. Total Environ.*, 2023, **875**, 162651.
32 Ž. Z. Tasić, M. B. P. Mihajlović, M. B. Radovanović, A. T. Simonović, D. V. Medić and M. M. Antonijević, *Sci. Rep.*, 2022, **12**, 5469.
33 B. N. Ferdousi, Md. M. Islam, T. Okajima and T. Ohsaka, *Electrochim. Acta*, 2007, **53**, 968–974.
34 S. F. Qin, F. F. Cheng, L. X. You and J. J. Sun, *Electroanal. Chem.*, 2022, **922**, 116788.
35 Md. S. Hossain, M. B. Mobarak, Md. F. Ahmed, U. S. Akhtar, M. S. Bashar and S. Ahmed, *Electrochim. Acta*, 2025, **521**, 145878.
36 G. K. Jayaprakash, B. E. Kumara Swamy, S. Rajendrachari and S. C. Sharma, *J. Mol. Liq.*, 2021, **334**, 116348.
37 T. Y. Lin and K. Y. A. Lin, *J. Taiwan. Inst. Chem. Eng.*, 2019, **96**, 321–328.
38 Y. Yardim, E. Keskin and Z. Senturk, *Talanta*, 2013, **116**, 1010–1017.
39 Y. L. Chen, W. Huang, K. J. Chen, T. Zhang, Y. Wang and J. M. Wang, *Talanta*, 2019, **196**, 85–91.

40 I. Vasilescu, S. A. V. Eremia, R. Penu, C. Albu, A. Radoi, S. C. Litescu and G. L. Radu, *RSC Adv.*, 2015, **5**, 261–268.
41 S. C. Fernandes, S. K. Moccelini, C. W. Scheeren, P. Migowski, J. Dupont, M. Heller, G. A. Micke and I. C. Vieira, *Talanta*, 2009, **79**, 222.
42 H. Zeiji, J. L. H. Cisneros, I. Naranjo-Rdriguez, B. H. Liu, K. R. Temsamani and J. L. Marty, *Anal. Chim. Acta*, 2008, **612**, 198–203.
43 M. L. D. Carvalho, M. Santhiago, R. A. Peralta, A. Neves, G. A. Micke and I. C. Vieira, *Talanta*, 2008, **77**, 394–399.
44 W. d. J. R. Santos, M. Santhiago, I. V. P. Yoshida and L. T. Kubota, *Anal. Chim. Acta*, 2011, **695**, 44–50.
45 M. Chao and X. Ma, *J. Food Drug Anal.*, 2014, **22**, 512–519.
46 I. G. David, D. E. Popa, M. Buleandra, Z. Moldovan, E. E. Iorgulescu and I. A. Badea, *Anal. Methods*, 2016, **8**, 6537–6544.